ENGINEERING JOURNAL

Article

Effects of Design Parameters on the Fluid Flow and the Efficiency of Single Ended Evacuated Tubular Solar Thermal Collectors via FEM Modelling and Experimentation

Junkun Ma[a] **and Cris Koutsougeras**[b,*]

Department of Computer Science & Industrial Technology, Southeastern Louisiana University, Hammond, LA 70402, USA
E-mail: [a]Junkun.Ma@selu.edu, [b]ck@selu.edu (Corresponding author)

Abstract. This work is about assessment of the single-ended evacuated tubular solar thermal collectors which are widely used in solar heating applications. Exchange and transfer of heat are accomplished by a thermosyphon process. The flow pattern of the working fluid within the collector is determined by a combination of gravity forces and the fluid's buoyancy forces which are due to varying density at varying temperature. This paper reports on a finite element method (FEM) based numerical study of the dependence of the working fluid flow pattern on the collector's design parameters such as inclination angles and collector length-to-diameter ratio. This fluid flow pattern determines the heat exchange between the working fluid and the selective coating and thus the efficiency of the collector. A model of this process has been implemented in a simulator built via the COMSOL FEM software package. A physical solar water heating system made with five commercial evacuated tubular collectors was also built and tested to verify the simulation results. Public access to the simulator is provided here.

Keywords: Tubular solar thermal collector, thermosyphon, solar heater efficiency, COMSOL simulation.

ENGINEERING JOURNAL Volume 19 Issue 5
Received 22 February 2015
Accepted 12 June 2015
Published 31 October 2015
Online at http://www.engj.org/
DOI:10.4186/ej.2015.19.5.69

DOI:10.4186/ej.2015.19.5.69

1. Introduction

Flat plate and evacuated tube collectors are the two most widely used solar thermal collectors for both domestic and commercial solar heating applications. Despite the long standing debate regarding the efficiency of the two collectors and the ISO 9806 standard [1] for testing solar collectors -according to which, efficiency could be measured in terms of gross roof area or absorber area- both theoretical [2–4] and experimental tests [5–7] have been presented that the evacuated tube collectors are more appropriate for high temperature applications such as steam production and regions with relatively long periods of overcastting sky and low ambient temperature.

Most evacuated tube collectors in the market use either a heat pipe design, [8] which is popular in Europe, or a direct flow design which is more popular in China. In the heat pipe design, an array of evacuated glass tubes -each holding a copper fin plate absorber fused to a copper heat pipe containing vaporizable fluid sealed in it- are connected to a manifold where heat is exchanged/transferred to other media such as water. Such a system is generally complicated by design, more expensive to manufacture and maintain, and heavy due to the copper plate and pipe use [9]. The direct flow evacuated tube collector uses a collector encased in dual layer glass tubes with vacuum in between the layers to eliminate heat loss due to conduction. The particular one that is the subject of this study is shown in Fig. 1 and has one end of the collector sealed with a layer of glazed coating and the other open end connected directly into a storage tank where the working fluid is stored. The open end and the storage tank is elevated with respect to the sealed end; as will be explained shortly, hot fluid medium rises to the tank whereas colder fluid sinks towards the sealed end of the tube(s). The selective absorbing coating on the outer surface of the inner tube absorbs and converts solar irradiation energy into heat and subsequently exchanges it to the working fluid by thermal conduction via the inner glass tube (Fig. 1 (b)).

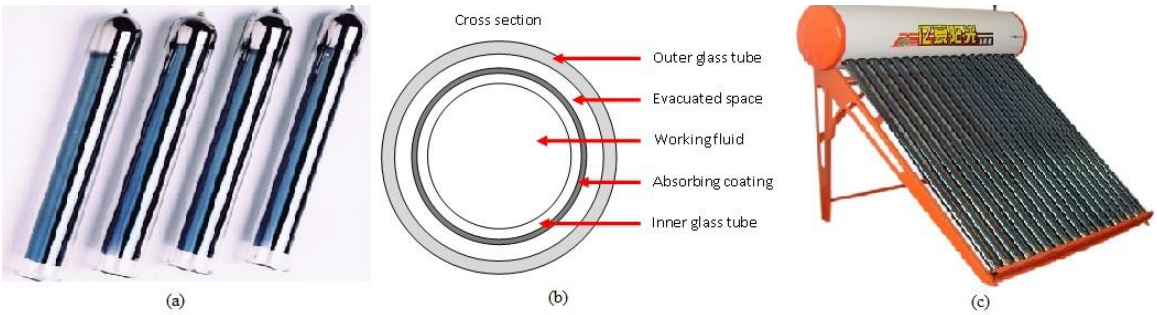

Fig. 1. (a) Single ended direct flow evacuated tube collector; (b) cross-section view; (c) solar water heater based on an array of singled ended direct flow evacuated tube collectors*.

Because of the circular geometry and the tilted installation setup, only the surface of the absorbing coating facing the sunlight irradiation will heat up and subsequently heats the adjacent working fluid. Under constant pressure, the density of the heated working fluid decreases and this causes the hotter fluid to float upward in the tube. Similarly, the working fluid with a lower temperature tends to move downward in the tube because of its relatively higher density.[10] The temperature gradient between the absorbing coating surface facing the sunlight and the opposite side generates heat flow and thus circulation of the working fluid within the inner glass tube.[11]

In the past, many works have dealt with the general issue of solar collector efficiency; some examples are listed in the references section[2–11] (but many more exist). The known works either provide performance assessments for specific configurations or specific products, or they provide modelling of various aspects of a tube collector system and the processes related to thermal transfer. The present work aims at building and making available a simulator [21] for an evacuated collector tube system. This paper reports the results of a study of the flow pattern of the working fluid within the inner tube of the direct flow evacuated tube collector using finite element methods (FEM). The main parameters on which to examine the dependence of the individual collector's efficiency are: (i) its tilted installation angle, (ii) the diameter of the inner tube, and (iii) the length of the collector. In addition, the effects of the installation distance between multiple collectors and relative incidence angle of the sunlight on the overall performance

* Courtesy of the Wuxi Wan Kang Solar Water Heater Co., Ltd. http://www.wktyn.com/

of a system are also discussed. Based on the analysis reported here, a COMSOL simulator was built and is available for further use by interested researchers. An experimental solar water heating system based on five such collectors provided by the Wuxi Wan Kang Solar Water Heater Co., Ltd. was also constructed and tested to verify the FEM simulation results. For the purpose of simplicity, water was the working fluid used in both simulation and experimental tests.

2. Thermosyphon Process of the Working Fluid within an Evacuated Tube Collector

The heating of the water within the collector involves two processes: heat conduction from the selective absorbing layer through the inner glass tube into the water, and fluid flow (natural convection) of the water. It is a thermal-fluid dynamics coupled multi-physics problem. The sun irradiation absorbing coating is considered to be the heat source of the collector (input), and the output is the net heat flux at the open end of the collector. The input energy flux from the absorbing coating is assumed to be a constant heat flux that is fed into the inner tube given that this work is focused on the effects of the aforementioned parameters of the collector's tilt and geometric dimensions. Due to the fact that only half of the coating is subjected to sun light at any given time, the heat flux input is assumed to come from the top half of the tube. Thus, the steady state heat conduction from the absorbing layer to the water is governed by an energy conservation equation [12]:

$$\rho C_p u \cdot \nabla T + \nabla \cdot (-k\nabla T) = Q \tag{1}$$

where $\boldsymbol{\rho}$ is fluid density, $\boldsymbol{C_p}$ is the heat capacity of the fluid, $\boldsymbol{u}$ is the velocity field of the fluid which is obtained from the Weakly Compressible Navier-Stokes equations, $\boldsymbol{\nabla}$ is the vector differential operator (gradient), $\boldsymbol{T}$ is the temperature of the fluid, $\boldsymbol{k}$ is the thermal conductivity of the fluid, and $\boldsymbol{Q}$ represents the heat source. As mentioned above, the steady state flow of the water within the inner tube is represented by the Weakly Compressible Navier-Stokes equations [13]:

$$\rho u \cdot \nabla u = \nabla \left[-pI + \eta(\nabla u + (\nabla u)^T) - \frac{2}{3}\eta(\nabla \cdot u)I\right] + F \tag{2}$$

$$\nabla(\rho u) = 0 \tag{3}$$

where $\boldsymbol{\rho}$ is the fluid pressure, $\boldsymbol{I}$ stands for the identity matrix, $\boldsymbol{\eta}$ is the fluid dynamic viscosity, the superscript $^{\mathrm{T}}$ denotes the transpose matrix, and $\boldsymbol{F}$ is the volumetric force which is the determining factor of the fluid flow pattern and it is the difference between the fluid's gravity and buoyancy.

To find the value of the volumetric force $\boldsymbol{F}$, a unit mass $\boldsymbol{M}$ of water with original volume $\boldsymbol{V}$ is considered. Suppose, for the moment, that the temperature of the water body that surrounds this unit mass $\boldsymbol{M}$ does not change (thus maintaining a constant density of $\boldsymbol{\rho}$), while the initial density $\boldsymbol{\rho}$ of the mass $\boldsymbol{M}$ (which is 'submerged' in the surrounding water of unchanged temperature) decreases to $\boldsymbol{\rho'}$ as its own temperature rises to a differential from its surrounding water body. Due to conservation of mass, the volume of the unit mass will increase from the original $\boldsymbol{V}$ to $\boldsymbol{V'}$ as shown in Fig. 2.

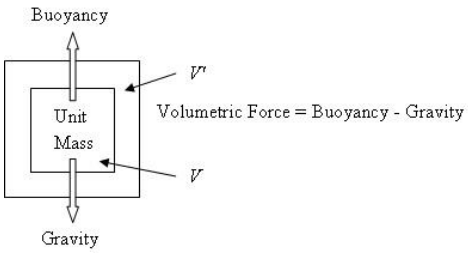

Fig. 2. Mechanical analysis of the volumetric force of unit mass water.

Based on the analysis above, the volumetric force per unit volume can be represented as:

$$F = \rho g (V' - V)/V = \rho g \Delta V/V \tag{4}$$

where $\boldsymbol{\rho}$ is the density of water, $\boldsymbol{g}$ is the gravitational force constant, $\boldsymbol{V}$ and $\boldsymbol{V'}$ are the initial and displaced volumes of the unit mass water. Since the fluid density and the gravitational force constant are constant at given temperature, the volumetric force is determined only by the value of $\boldsymbol{\Delta V/V}$.

In terms of volume, the coefficient of thermal expansion (CTE) of materials is defined as the ratio between changes in volume in response to changes in temperature of the materials as:

$$\alpha = (\Delta V/V)/\Delta T \text{ or } \Delta V/V = \alpha \Delta T \tag{5}$$

DOI:10.4186/ej.2015.19.5.69

Combining Eq. 4 and Eq. 5, the volumetric force per unit volume of the water can be represented as:

$$F = \rho g \alpha \Delta T \quad (6)$$

3. Numerical Implementation

The above theoretical framework was then used to perform simulations using COMSOL as explained in the following sections. The COMSOL Multiphysics simulation environment was used for this study because of its available predefined heat transfer and fluid dynamics interfaces and because of the easiness to couple them together for multiphysics simulation [14]. In addition, its interface allows input of user defined terms such as the volumetric force of Eq. 6 and this simplifies the process of modifying the governing constitutive equations such as Eq. 2.

3.1. FEM Model

Since the outer glass tube of the collector is mainly for creating a vacuum layer between itself and the inner glass tube and the heat transfer and fluid flow physics of our interest take place in the inner tube, it is only necessary to model and simulate the two physics at the inner tube. Based on measurement of the actual collector used for experimental tests and specifications supplied by the manufacturer [15] the geometry of the collector is modelled to be 1200mm long, 47mm inner diameter, with inner glass tube thickness of 2.5mm as shown in Fig. 3.

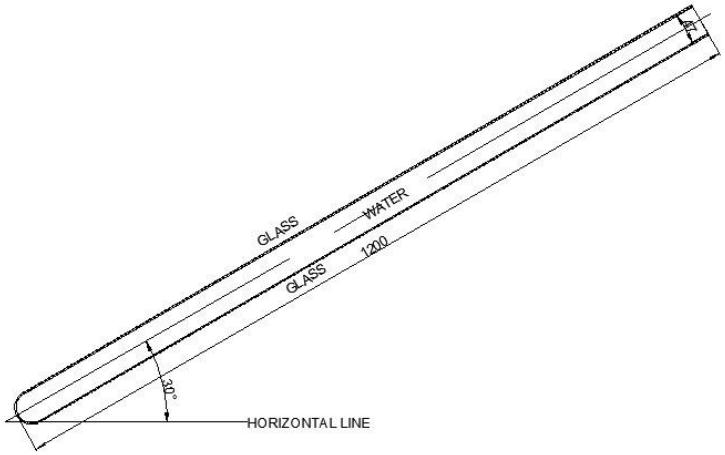

Fig. 3. Model of a single ended evacuated tube collector tilted at 30º.

Since the open end of the collector is connected directly to a storage tank, this opening serves as both the inlet for cold water to enter the collector (via the lower portion of the opening) and the outlet for hot water to exit (via the upper portion of the opening) the collector, the upper and lower half of the open end of the collector are modelled as outlet and inlet respectively as shown in Fig. 4.

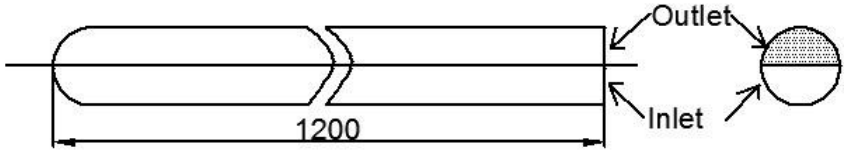

Fig. 4. Outlet and inlet assumption for the open end of the collector.

In addition, the following assumptions were made for the simulation: 1) thermal expansion of the glass tube is ignored as being very small to be of any significant consequence; 2) ambient temperature is 298.15 Kelvin [25ºC] and the system collector is subjected to 1 atmospheric pressure; 3) the properties of water are based on that of the pure water at 0.01ºC [16]; 4) the properties of glass are based on that of borosilicate glass used to manufacture the collector used in experimental tests[17]; 5) the effects of the water tank and other accessories are ignored.

3.2. Efficiency Calculation

Suppose a certain amount of water with mass $\boldsymbol{M}$ goes into tube collector from the inlet with an initial temperature of $\boldsymbol{T_0}$ and comes out of the collector from the outlet with a final temperature of $\boldsymbol{T}$ after being heated over a certain period of time $\boldsymbol{t}$. Then, the energy gain of this body of water can be represented as:

$$\Delta Q = C_p M(T\text{-}T_0) = C_p \rho V \Delta T \quad (7)$$

where $\boldsymbol{\Delta Q}$ is the energy gain, $\boldsymbol{C_p}$ is the specific heat capacity of water, $\boldsymbol{\rho}$ is the density of the water, $\boldsymbol{V}$ is the volume of the water, and ΔT is the temperature difference after the body of water circulating through the collector. If we rewrite Eq. (7) in power format, it becomes:

$$P = \Delta Q/t = C_p(M/t)(T\text{-}T_0) = C_p \rho (V/t)\Delta T \quad (8)$$

The ratio between this calculated power and the input from the absorbing coating determines the efficiency of the collector. To calculate the power $\boldsymbol{P}$ in Eq. (8), we still need to find the volume of water which flows through the collector within a given time $\boldsymbol{t}$, and the temperature difference $\boldsymbol{\Delta T}$ of this water when it goes in and when it comes out of the collector. Because both the velocity and temperature vary within the whole volume of water in the collector, integration over the surface of the outlet boundary was applied.

In order to compute the net energy flowing through a cross section of a flow, we need to integrate the energy of the fluid over the cross-section area (surface). The reason is that the velocity of the fluid is not constant over the entire cross section of the outlet area. Consider a representative surface area $\boldsymbol{dA}$ on the outlet. Since only the velocity component of the fluid flowing along the normal direction of the outlet surface will generate net flow, the normal velocity at this area can be expressed as:

$$n \cdot U = n_x{*}u + n_y{*}v + n_z{*}w \quad (9)$$

where $\boldsymbol{n}$ is the normal vector of the outlet, $\boldsymbol{U}$ is the velocity vector of the water at the outlet, $\boldsymbol{n_x}$, $\boldsymbol{n_y}$, and $\boldsymbol{n_z}$ are the unit vectors along the X, Y, and Z coordinate axes respectively, and $\boldsymbol{u}$, $\boldsymbol{v}$, and $\boldsymbol{w}$ are the three velocity components along the X, Y, and Z coordinates. Similarly, the temperature difference can be expressed simply as $\boldsymbol{T\text{-}T_0}$, where $\boldsymbol{T}$ is the temperature of the water exiting the area and $\boldsymbol{T_0}$ is the temperature of the fluid entering the collector from the inlet. Integrating this net flow multiply the temperature difference over the outlet surface, the power $\boldsymbol{P}$ in Eq. (8) can be obtained.

$$P = C_p \rho \oint (n_x{*}u + n_y{*}v + n_z{*}w)(T\text{-}T_0)dA \quad (10)$$

3.3. Studied Parameters

The model was setup in the COMSOL FEM package and experimentation via simulations was conducted. In these simulations, some design parameters of interest were varied in order to understand how the efficiency of the collector is affected. These parameters include the installation angle of the collector, physical dimension of the collector, and the distance between neighboring collectors in an array of these collectors.

3.3.1. Installation angle

The first and also the main factor affecting the collector's efficiency is the installation angle. Since the collector is generally installed at a certain tilted angle with respect to the horizontal plane, the gravity of water can be divided into two components: the one parallel to the tube and the other perpendicular to the tube. The magnitude of each component is determined by the tilted installation angle as shown in Fig. 5. The two component forces can potentially impede or facilitate the natural thermal convection of the water within the collector and thus the overall efficiency of the collector. In this study, mounting angles starting from 15^0 with an increment of 5^0 until 75^0 were modeled and an experimental system detailed in section 4 has also been fabricated and tested to verify the modeling results.

3.3.2. Physical dimensions of the collector

In considering the physical dimensions of the collector tube, the length to diameter ratio was also investigated. A short survey of commercially available collectors shows that there are many mass produced single ended evacuated tube collectors with different dimensional specifications. In this study, collectors

DOI:10.4186/ej.2015.19.5.69

with identical 47mm inner diameter but length ranging from 1200mm to 1800mm with an increment interval of 50mm are modelled to check the effects of aspect ratio (ratio between collector length and inner tube diameter) on the collector's efficiency.

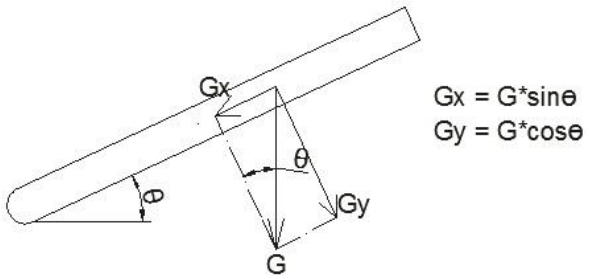

Fig. 5. Two components of the gravitational force of the water.

3.3.3. Spacing of the collectors.

In most solar heating systems based on this type of collector, there is usually an array of these collectors installed parallel to each other. When the sunlight incidence is 90^0 as shown in Fig. 6(a), each collector has half of the absorbing coating subjected to sunlight. If the sunlight incidence is some value other than 90^0 as shown in Fig. 6(b), the outmost collector tube will still have half of the coating surface exposed to the sunlight, but all other collector tubes will expose less absorbing area due to shading. Suppose the sunlight is maintained at a fixed angle, the gap between tubes is directly related to the size of the blocked/shaded area as shown in Fig. 7. Therefore, the tube spacing in the collector array affects the overall efficiency of these collectors. In this study, models consisting of two collector tubes with distance between them ranging from 10mm to 50mm at the increment of 5mm were created to investigate this effect. The sunlight incidence is fixed at 30^0 in these models.

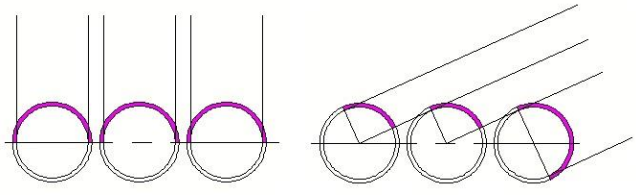

Fig. 6. Two different sunlight incidences.

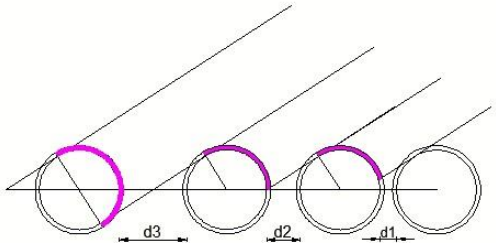

Fig. 7. Space between collectors and its effects on absorbing area.

4. Experimental Tests

A solar water heating system was constructed as shown in Fig. 8 to experimentally test the effects of installation angle on the efficiency of the collectors. This system was made with five single ended evacuated solar thermal collectors (1200mm long with 47mm inner tube diameter) that are connected to a PVC pipe (1500mm long with 152.4mm inner diameter) functioning as water storage tank. The collectors in the system are placed in such a way so that the spaces between all collectors will not cast shadows on nearby collectors for an incidence angle smaller than 60^0.

DOI:10.4186/ej.2015.19.5.69

Fig. 8. A solar water heating system with five single ended evacuated solar thermal collectors.

The system is filled with 25 liters of tap water and then set in sunlight for one hour at varying tilted angles. Each of these experiments was started with both the system and its water initially at room temperature. To ensure a constant sunlight irradiation between all tests, the experiments were carried out around noon time during sunny days without clouds. Sunlight intensity during the tests was measured every 15 minutes using a portable light intensity meter for each test [18]. Table 1 shows the measured sun light intensity values during the experiment tests with the average and variation range shown in Fig. 9. The average measured sunlight intensity is 1278 W/m² with a variation range of approximately 50W/m², which is less than 4%, during all the tests.

Table 1. Measured sunlight intensity during the experiments.

Tilt Angle		Measured Sunlight Intensity (W/m^2)					Average	Lower	Upper
(degrees)		1	2	3	4		(W/m^2)	(W/m^2)	(W/m^2)
15		1284.5	1279.7	1290.2	1288.5		1285.7	6.0	4.5
20		1249.3	1255.4	1260.3	1258.5		1255.9	6.6	4.4
25		1266.3	1270.0	1271.4	1259.2		1266.7	7.5	4.7
30		1276.1	1270.5	1283.1	1281.3		1277.8	7.3	5.3
35		1277.5	1285.4	1284.3	1279.5		1281.7	4.2	3.7
40		1269.1	1280.5	1277.6	1281.3		1277.1	8.0	4.2
45		1277.5	1285.7	1288.4	1279.3		1282.7	5.2	5.7
50		1298.5	1291.4	1294.5	1287.8		1293.1	5.3	5.5
55		1279.8	1288.5	1286.4	1285.8		1285.1	5.3	3.4
60		1266.5	1269.5	1261.5	1259.9		1264.4	4.4	5.2
65		1277.2	1290.5	1275.6	1288.4		1282.9	7.3	7.6
70		1267.8	1284.3	1277.6	1285.6		1278.8	11.0	6.8
75		1289.5	1279.6	1288.4	1269.5		1281.8	12.3	7.8
						Min	1255.9		
						Max	1293.1		
						Average	1278.0		

DOI:10.4186/ej.2015.19.5.69

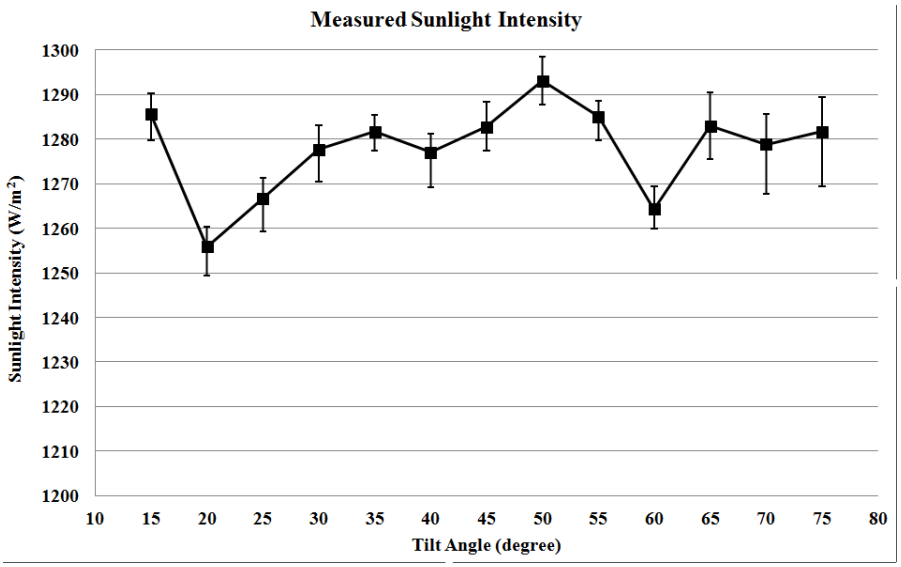

Fig. 9. Measured sunlight intensity during experimental tests.

The efficiency of the system was obtained by calculating the ratio of the energy absorbed by the water in the form of heat to that of the sunlight radiation on the selective absorbing coating. The heat absorbed by the water can be simply derived from the temperature change of the water in the tank over the one hour testing period of time.

$$Q = MC_p\Delta T \tag{11}$$

where $\boldsymbol{Q}$ is the total heat water absorbed, $\boldsymbol{M}$ is the mass of the water, $\boldsymbol{C_p}$ is the heat capacity of the water, and ΔT is the water temperature change of the water over the one hour testing period. The input from sunlight is calculated as the sun flux that hits the absorbing area (area of the coating on the collector tube that is subjected to sunlight irradiation). A converting efficiency of 90% for the selective absorbing coating is chosen based on results reported by other researchers [19, 20]. Table 2 shows the experimentally measured results. The mass of the water in the system was obtained from the volume of water in the system. The initial and final temperatures of the water were measured using a thermocouple probe inserted into the PVC tank. Based on the total amount of energy exchanged to the water in the system, the average power of the system over the one hour testing period was calculated.

Table 2. Experimentally measured results for different tilt angles.

Mass (Kg)	Initial Temp (^{0}C)	Final Temp (^{0}C)	Delta Temp (^{0}C)	Heat Absorbed (J)	Measured Power (W)
25.0	27.6	42.8	15.2	1591536.4	442.1
25.0	25.8	41.4	15.6	1627113.1	452.0
25.0	24.5	40.8	16.3	1706637.6	474.1
25.0	25.5	41.8	16.3	1701405.8	472.6
25.0	29.6	45.3	15.7	1642808.8	456.3
25.0	27.6	43.2	15.7	1640716.0	455.8
25.0	23.9	39.5	15.6	1631298.6	453.1
25.0	28.6	44.2	15.6	1630252.3	452.8
25.0	27.6	42.7	15.1	1576887.1	438.0
25.0	27.1	42.2	15.1	1574794.4	437.4
25.0	25.7	39.8	14.0	1469110.5	408.1
25.0	27.5	41.9	14.4	1502594.5	417.4
25.0	29.6	43.9	14.3	1499455.4	416.5

Since the calculated power is a time average over the one hour testing period, environmental conditions such as ambient temperature and wind speed could affect the heat loss, which will affect the experimental results. Figure 12 shows such a variation but the trend still agrees with the simulated results.

5. Results and Discussion

The fluid dynamics and heat transfer of the water within the collector were successfully simulated using COMSOL Multiphysics. Figure 10 shows a snap shot of the temperature distribution and the flow stream lines of the water within the collector tube. It can be seen clearly that the temperature of the upper portion of the water adjacent to the upper surface of the collector tube where the absorbing coating is subjected to sunlight irradiation rises, while the temperature of the lower portion of the water near the back side of the absorbing coating shaded by the tube itself remains relatively low. The stream line shows that the water does circulate from the open end all the way down to the sealed end of the collector.

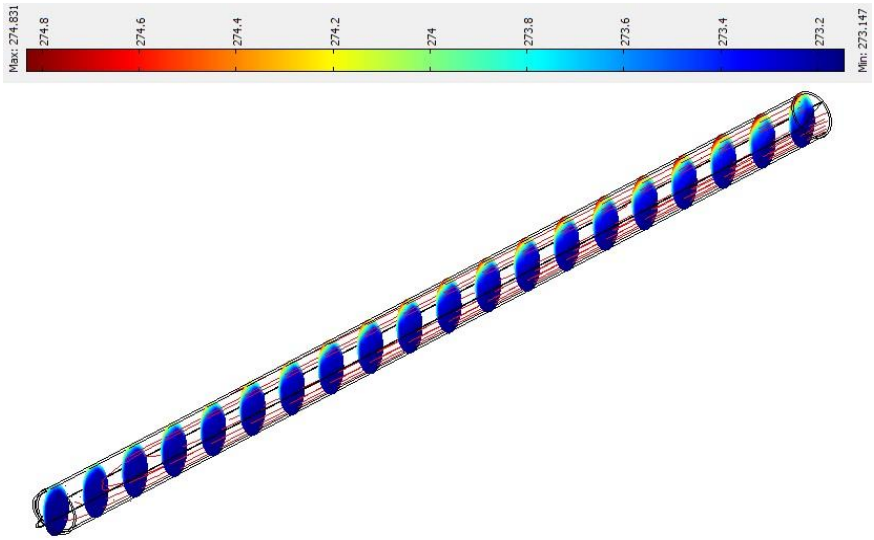

Fig. 10. Temperature distribution and stream line of water flow.

A center cross section of the collector with the water temperature and velocity field distributions is shown in Fig. 11. The results suggest that the water at the bottom of the collector is heated and starts to rise. It is further heated as it is rising towards the elevated open end and reaches maximum temperature when it exits the collector. It is also noticed that the velocity of the water decreases as it is moving downward towards the sealed end of the collector.

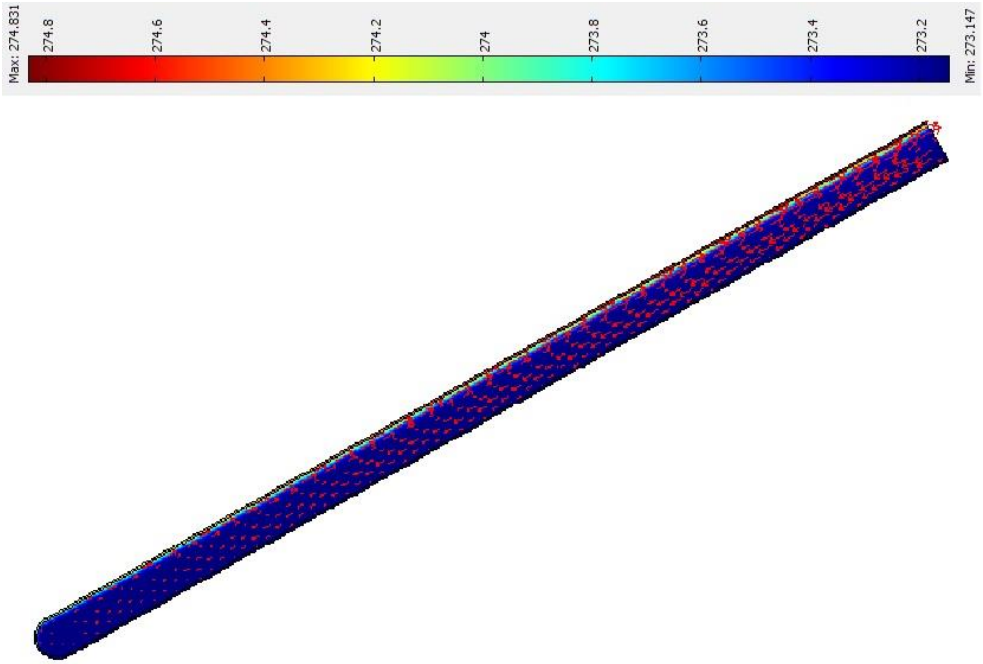

Fig. 11. Center cross section showing temperature distribution and velocity field of the water.

DOI:10.4186/ej.2015.19.5.69

Tilt Angle	Simulation	Experiment
(degrees)	(W/m^2)	(W/m^2)
15	1069.1	998.3
20	1120.8	1020.5
25	1135	1070.2
30	1129.9	1066.8
35	1113.3	1030.5
40	1098.3	1029.2
45	1085.7	1023.0
50	1072.2	1022.3
55	1060.6	988.6
60	1049.4	987.5
65	1036.6	921.2
70	1031.8	942.4
75	1023.1	940.2

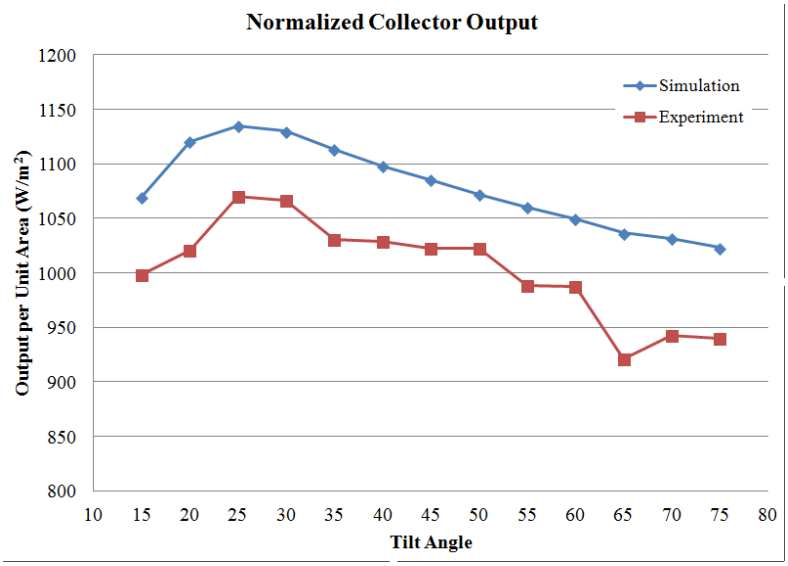

Fig. 12. Collector power per unit absorbing coating area for different tilted install angle.

As described in section 4, the sunlight intensity for the experimental tests was measured to be an average value of 1278W/m². Considering the converting efficiency of the absorbing coating, the heat flux entering the collector inner tube is set to be 1150W/m² in all simulations. The simulation results were compared to the experimental ones for understanding the effects of the tilted installation angle on performance of these collectors. Since the model simulation is for only one collector tube and the experimental system is made out of five collector tubes, the power output of the collector as shown in Table 2 was normalized to per unit absorbing coating area by dividing the experimentally measured power by the total absorbing area of the experimental system. Figure 12 shows the comparison of the simulation and experimental test results.

From the chart, it can be concluded that the collector works most efficiently when the tilted install angle is approximately 25^0. One aspect that needs to be pointed out is that the experimental results show 10%~15% less output compared with that of the simulation for all tilted angles. This phenomenon is likely the combined effects of inconsistent sunlight intensity as described in section 4, the PVC storage tank, the fittings connecting the collector to the storage tank, and heat losses from the fitting and the storage tank to the ambient during the tests - although they were all thermally insulated with fiberglass materials.

Inner Tube Diameter 47mm		
Tube Length		Simulation
(mm)	(m)	(W/m^2)
1200	1.2	1130.9
1250	1.25	1130.5
1300	1.3	1134.7
1350	1.35	1135.0
1400	1.4	1136.8
1450	1.45	1136.8
1500	1.5	1138.0
1550	1.55	1137.6
1600	1.6	1135.4
1650	1.65	1134.2
1700	1.7	1132.4
1750	1.75	1128.8
1800	1.8	1128.7

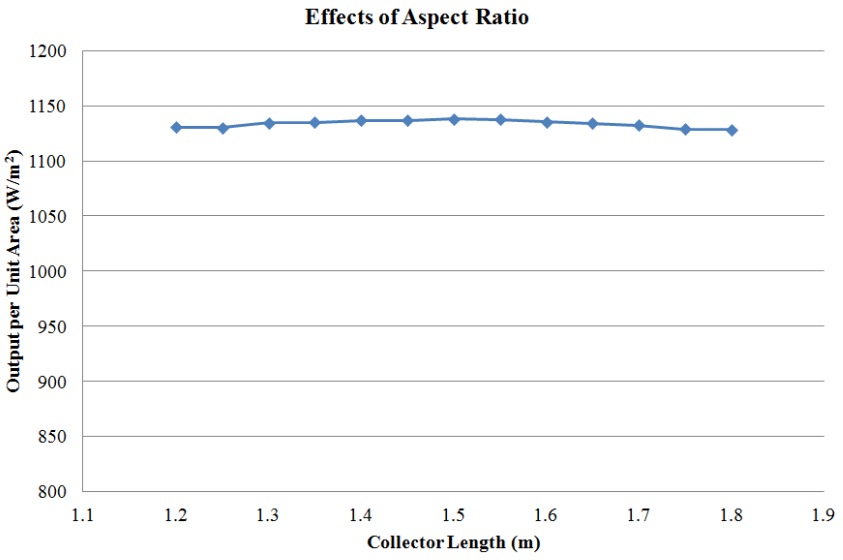

Fig. 13. Collector power per unit absorbing coating area for different collector length.

As described in section 3.3, the effects of the length to inner diameter ratio of the collector tube on its efficiency were also studied. Since different length results in different absorbing coating area, the output of

the collector was also normalized. For the purpose of comparison, the scale of the normalized output for collectors with different length was kept the same as that in Fig. 12 and shown in Fig. 13. According to these simulations, it does not appear that the aspect ratio between collector length and inner tube diameter has any significant effect on the performance of the collector; in comparison the tilt angle appears to be the most dominant.

In case of multi-tube systems, to avoid possible shading which blocks neighboring collector tube and thus reduces total absorbing coating area, it is necessary to set up a minimum distance between tubes. In the scenario described in section 3, simple geometry analysis shows that a minimum of 50mm space is required between collector tubes for a minimum sunlight incidence angle of 30^0. However, this will increase the total area requirement for the whole system which is a limiting factor in practice.

The source files of the COMSOL simulations that were developed for this work are available on the internet [21]. They should be useful to interested researchers for further research and for estimation/verification of any desired custom modifications. The source files can be easily modified in order to quickly obtain custom simulations for any desired change of the system's physical parameters.

6. Conclusions

A FEM numerical model was discussed for modelling the thermosyphon process and the efficiency of single-ended evacuated tubular solar thermal collectors. COMSOL Multiphysics successfully simulated the coupled heat transfer and thermal convection of the water within the inner glass tube of the single ended evacuated tube solar thermal collector. It was concluded by both the simulations [21] and experimental results that the selected collector reaches its peak efficiency when its tilted installation angle is approximately 25^0. Based on per unit area of absorbing coating, the aspect ratio between the collector length and inner tube diameter has minimum effects on the performance of the collector. Near optimal spacing between adjacent collectors is 50mm but should be chosen on a case by case basis since larger space increases the total surface area required for a multi-collector system.

References

[1] *ISO 9806-2:1995. Test Methods for Solar Collectors—Part 2: Qualification Test Procedures*, International Organization for Standardization, Geneva, Switzerland.

[2] S. Arora, S. Chitkara, R. Udayakumar, and M. Ali, "Thermal Analysis of evacuated solar tube collectors," *Journal of Petroleum and Gas Engineering*, vol. 2, no. 4, pp. 74–82, 2011.

[3] J. Praene, F. Garde, and F. Lucas, "Dynamic modelling and elements of validation of solar evacuated tube collectors," presented at *Ninth International IBPSA Conference*, Montreal, Canada, 2005.

[4] L. Ma, Z. Lu, J. Zhang, and R. Liang, "Thermal performance analysis of the glass evacuated tube solar collector with U-tube," *Building and Environment*, vol. 45, no. 9, pp. 1959–1967, 2010.

[5] E. Zambolin, D. Del Col, "Experimental analysis of thermal performance of flat plate and evacuated tube solar collectors in stationary standard and daily conditions," *Solar Energy*, vol. 84, no. 8, pp. 1382–1396, 2010.

[6] I. Budihardjo and G. L. Morrison, "Performance of water-in-glass evacuated tube solar water heaters," *Solar Energy*, vol. 83, no. 1, vol. 49–56, 2009.

[7] M. Hayek, A. Johnny, and L. William, "Experimental investigation of the performance of evacuated-tube solar collectors under Eastern Mediterranean climatic conditions," *Energy Procedia*, vol. 6, pp. 618–626, 2011.

[8] S. Fischer, "Performance testing of evacuated tubular collectors," Quality Assurance in Solar Heating and Cooling Technology, 2012.

[9] F. Mahjouri, (2005). Vacuum Tube Liquid-Vapor (Heat-Pipe) Collectors. [Online]. Available: http://www.thermomax.com/Downloads/Vacuum%20Tube%20Paper.pdf

[10] C. Chang, T. Lin, and W. Yan, "Natural convection flows in a vertical, open tube resulting from combined buoyancy effects of thermal and mass diffusion," *International Journal of Heat and Mass Transfer*, vol. 29, no. 10, pp. 1543–1552, 1986.

[11] I. Budihardjo and G. L. Morrison, "Natural circulation flow through water-in-glass evacuated tube solar collectors," *Solar Energy*, vol. 81, no. 12, pp. 1460–1472, 2007.

[12] *Heat Transfer by Free Convection*, *COMSOL® Version 3.5a Handbook*, 2010.

[13] *The CFD Module Interfaces*, *COMSOL® Version 3.5a Handbook*, 2010.
[14] K. David. Multiphysics Simulation with COMSOL On-Demand Webinar. [Online]. Available: http://www.engineering.com/ResourceDownload/MultiphysicsSimulationswithCOMSOLWebinar.aspx
[15] Wuxi WanKang Solar Water Heaters Co. Ltd. Heat Pipe Solar Collector. [Online]. Available: http://www.wksolar.com/products/solar-collector/heat-pipe-solar-collector-wcd
[16] The Engineering ToolBox, (2010). Water-Thermal Properties. [Online]. Available: http://www.engineeringtoolbox.com/water-thermal-properties-d_162.html
[17] Pegasus, (2010). Technical Information. [Online]. Available: http://www.pegasus-glass.com/Portals/0/technical_info.pdf
[18] M. Iqbal, *An Introduction To Solar Radiation*. Academic Press, 2012.
[19] N. Sergeant, M. Agrawala, and P. Peumansa, "Design of selective coatings for solar thermal applications using sub-wavelength metal-dielectric structures," in *Proc. of SPIE Solar Energy+ Technology*, 2009, p. 74100C.
[20] N. Ehrmann and R. Reineke-Koch, "Selectively coated high efficiency glazing for solar-thermal flat-plate collectors," *Thin Solid Films*, vol. 520, no. 12, pp. 4214–4218, 2012.
[21] J. Ma and C. Koutsougeras. COMSOL Simulator for Solar Water Heaters. [Online]. Available: http://www2.selu.edu/Academics/Faculty/ck/Comsol_Evacuate_Tube_Ma_Koutsougeras_2014